J. Fluid Mech. (2006), *vol.* 555, *pp.* 387–408.
doi:10.1017/S0022112006009517 Printed in the United Kingdom

The far downstream evolution of the high-Reynolds-number axisymmetric wake behind a disk. Part 2. Slice proper orthogonal decomposition

By PETER B. V. JOHANSSON AND WILLIAM K. GEORGE

Turbulence Research Laboratory, Department of Applied Mechanics, Chalmers University of Technology, Gothenburg, SE-412 96, Sweden

(Received 22 November 2004 and in revised form 4 November 2005)

The high-Reynolds-number axisymmetric wake behind a disk has been studied from $x/D = 30$ to $x/D = 150$ using the proper orthogonal decomposition (POD) applied to measurements of the streamwise fluctuating velocity. It was found that the energetic structure of the axisymmetric wake can very efficiently be described in terms of POD modes. The first radial (or lowest-order) POD mode has 56 % of the energy. Two major features dominate the eigenspectra, manifested as two major peaks. The first peak is an azimuthal mode-1 peak at a frequency corresponding to the Strouhal number of the near wake. The second is an azimuthal mode-2 peak at near-zero frequency. The mode-1 peak dies out faster than the mode-2 peak, so that the far wake is dominated by the latter.

This evolution from azimuthal mode-1 dominance in the near wake to mode-2 dominance in the far wake corresponds closely to the approach to equilibrium similarity. Once azimuthal mode-2 becomes equally important as azimuthal mode-1 (after $x/D = 30$ or $x/\theta = 110$), the ratio of turbulence intensity to centreline velocity deficit is constant, the mean deficit and turbulence intensity collapse in similarity variables, and the wake grows as $x^{1/3}$.

1. Introduction

The structure of the three-dimensional wake was perhaps first studied by Marshall & Stanton (1931). They presented photographs of wakes behind circular disks in water. The dye trace revealed an unsteady pattern when the Reynolds number based on the free-stream velocity and disk diameter, Re, exceeded about 200. They also concluded that there was a periodic shedding of ring vortices. The sphere wake was also studied by flow visualization in a water tank by Möller (1938), who found a spiral vortex in the wake in a certain range of Reynolds numbers.

Flow visualization experiments were performed on low-Reynolds-number wakes by Magarvey & Bishop (1961) who studied falling drops up to $Re = 2500$. They used dye visualization techniques to study the vortex structure of the wake, and attempted to describe the mechanisms of transition and to provide limits for when the flow undergoes transition from laminar to turbulent flow. This study was followed by Magarvey & MacLatchy (1965), who studied falling spheres for $Re < 500$, and attempted to describe the manner in which vortices are released into the free stream.

The vortex structure for a sphere wake at a higher Re was studied by Pao & Kao (1977). They investigated wakes with Re up to 2×10^4. The main findings were that without stratification, vorticity was shed three-dimensionally, and that stable stratification resulted in the wake collapsing. Based on their observations, they modelled the vortex configuration in the wake.

The sphere wake was later studied by Taneda (1978), who used the surface oil-flow method, smoke visualization and a tuft-grid to visualize the flow for Re up to 10^6. He showed evidence that the wake performed a wave-like motion up to $Re = 3.8 \times 10^5$, and that it forms a pair of streamwise vortices at higher values of Re.

An experimental and analytical investigation of the stability of the axisymmetric wake was made by Sato & Okada (1966), who studied a slender axisymmetric body of revolution. Analytically, they applied the criterion of Batchelor & Gill (1962) to their laminar wake velocity profile, and concluded that according to this criterion, azimuthal modes 1 and 2 could possibly be unstable. They were not able to numerically find a solution for mode-2, and their experimental data were found to be in agreement with mode-1 as the only unstable mode. The stability of the axisymmetric wake was also investigated theoretically by Monkewitz (1988), who expanded previous studies by investigating a family of wake velocity profiles. He confirmed previous conclusions that azimuthal mode 1 was the most unstable, and in fact the only one that can trigger absolute instability of this flow.

Numerically, the transition was studied by Kim & Pearlstein (1990), who studied linear stability using a spectral technique to create a base flow that was disturbed by axisymmetric and non-axisymmetric disturbances. Their main finding was that azimuthal mode 1 was the most unstable. This was followed up by Natarajan & Acrivos (1993), who used finite-element methods to numerically study the transitional stages of spheres and disks. They did not agree with Kim & Pearlstein (1990) on the manner in which the wake passes through the initial stages of transition, but they confirmed the conclusion that mode-1 was the most unstable. This was also found by Tomboulides & Orszag (2000) as well as by Ghidersa & Dušek (2000).

The temporal linear parallel stability theory of Batchelor & Gill (1962) has recently been re-visited by George, Johansson & Gamard (2002), who found that the conclusion of Batchelor & Gill (1962) that azimuthal mode-1 is the only possible unstable mode directly related to the particular choice of the mean velocity profile. Indeed, the profile selected by Batchelor & Gill (1962) only allows mode 1 to be unstable, but the same analysis applied on a more realistic profile for the far jet or wake reveals that azimuthal modes 0, 1, and 2 can be unstable.

Johnson & Patel (1999) investigated the flow behind a sphere at low Reynolds number numerically and experimentally. They proposed a symmetry-breaking mechanism to advance the basic understanding of the steady, non axisymmetric regime between $Re = 210$ and 270. At $Re = 300$, a highly organized periodic flow was found that was dominated by vortex shedding.

The large-scale, 'coherent' features of this flow have not only been studied using flow visualization, but also by means of phase averaging and conditional sampling techniques (Lee & Bearman 1992; Miau *et al.* 1997; Perry & Lim 1978; Perry & Watmuff 1981). Most interestingly in the context of this paper, Roberts (1973), and later Fuchs, Mercker & Michel (1979) used two hot wires to measure cross-spectra at a single radius of the near wake. Fuchs *et al.* (1979) varied the angular separation of the probes and were able to decompose the cross-spectra into Fourier modes. The azimuthal modal content was then studied at the frequencies that were found to be eventful. At $x/D = 9$, they found a strong azimuthal mode-1 peak at a frequency corresponding to the vortex shedding frequency, but also a peak for mode-2 at very

low frequencies. The mode-1 peak was clearly dominant. Berger, Scholz & Schumm (1990) also conducted a similar investigation, and reported a dominant mode-1 peak. They did not mention mode-2, even though it is clearly present in their results.

Subsequently, Cannon, Champagne & Glezer (1993) investigated the axisymmetric wake, in part by means of flow visualization. They showed that the wakes from five different wake generators (sphere, disk, and three screens of different porosity) behaved very differently. They also performed an azimuthal decomposition of the velocity field at a fixed radius of the wake at $x/\theta = 105$ for the disk and one of the screens, and concluded that azimuthal mode-1 was the dominating feature. They further suggested this might be connected to the vortical structures seen in the flow visualization photographs. They also noted that these vortical structures were still present at considerable downstream distances.

The proper orthogonal decomposition (POD) is in essence a structured way of organizing the azimuthally transformed cross-spectra. Originally introduced to the field of turbulence by Lumley (1967), the POD has been applied to many flows. One recent example is to the plane mixing layer by Bonnet *et al.* (1998), where different techniques of eddy structure identification methods were compared. This role of the POD was further discussed in detail by Delville *et al.* (1999). The 'slice' version of the POD technique was first applied to the jet mixing layer by Glauser (1987), Glauser & George (1987), Citriniti & George (2000) and Jung, Gamard & George (2004) and to the far jet by Gamard *et al.* (2002) and Gamard, Jung & George (2004). The last three are of special interest, since in many ways their findings parallel the results of this paper.

Johansson, George & Woodward (2002) recently investigated the near wake of a disk (to $x/D = 50$) using the 'slice' POD technique. It was found that azimuthal mode-1 dominated the eigenspectra until $x/D = 10$. This was not surprising in view of the many earlier investigations. After this position, however, the magnitude of both modes decreased, but azimuthal mode-1 fell much more rapidly than azimuthal mode-2. They were equally important at $x/D = 30$, after which the dominance was taken over by mode-2. The emergence of and eventual dominance of mode-2 was not expected. No theories had predicted this, nor had azimuthal mode-2 ever been observed to be of significance experimentally. Similar behaviour was observed, however, almost simultaneously in the high-Reynolds-number axisymmetric jet by Gamard *et al.* (2002) and subsequently in the low-Reynolds-number DNS of the same flow (Freund & Colonius 2002).

Our previous experiments (Johansson *et al.* 2002) were carried out in the Chalmers wind tunnel. In view of the surprising nature of the results and their theoretical implications, it was deemed highly desirable to repeat the experiments in a longer facility of superior flow quality. The results reported here extend those of the earlier study downstream a factor of three. Also several additional studies were made to evaluate the effects of array coverage, number of probes, and the manner in which the disk is suspended in the flow. These are included in Appendix A.

2. Experimental setup

The experiment was performed in the MTL wind tunnel at the Royal University of Technology (KTH) in Stockholm, Sweden. The experimental setup and single point flow characterization are described in Part 1 (Johansson & George 2006). Detailed characteristics of the tunnel can be found in Johansson (1992). Here, only the issues directly related to the POD are discussed herein.

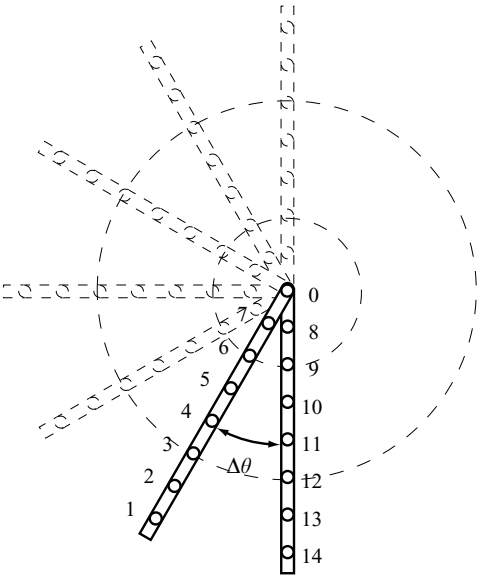

FIGURE 1. Map of traverse scheme, shown in increments of $\Delta\theta = 30°$. Our experiment had $\Delta\theta = 15°$.

2.1. *Disk suspension*

The disk used in the experiments had a diameter of 20 mm, was made of acrylic and was suspended with three pairs of wires, each of diameter 0.2 mm. The disk was placed 1 m into the measuring section to allow probe calibration upstream of the disk. Previous experiments reported by Johansson *et al.* (2002) used four support wires instead of three, and a discussion about differences in the final result is found in Appendix B. There were none observed.

2.2. *Spatial resolution*

The arrays were used in the same manner as Glauser & George (1987) and Johansson *et al.* (2002) to obtain the two-point velocity cross-spectra for all combinations of locations shown in figure 1. The measurement grid of 7×7 was chosen following Glauser & George (1992), so as to provide the minimal resolution to apply the POD. In order to avoid spatial aliasing, the number of azimuthal measurement positions must be greater than the number of modes needed to describe the energy in the flow. Similar considerations apply in the azimuthal direction where the number of angular increments must be greater than twice the number of azimuthal modes required (since these eigenfunctions are in general complex), which for this experiment was estimated as 12.

The maximum radius of the rakes is also important, and must span enough of the flow so that the POD results are independent of it. Since the rake is fixed but the wake grows, the relative coverage varies downstream. Appendix A contains an evaluation of the effects of varying coverage on the results reported below. The effect is very small for the range of variation in these experiments.

The upper array of probes was movable, and traversed from a 15° separation up to 180° with 15° increments in $\Delta\theta$, see figure 1. Each hot-wire probe is numbered and marked by a circle. The angular separation $\Delta\theta = 90°$ could not be measured directly, since the movable probe rake caught the wake of the suspending wires. Instead,

measurements at the opposite position 270° were used. In all, half the cross-section of the wake at a fixed downstream position was scanned, and pairs of instantaneous velocity cross-spectra were computed for a fixed angle separation. Note that the cross-spectra corresponding to the remaining half-plane were available from the azimuthal symmetry of the flow, which was in turn verified through the extensive tests reported in Part 1.

3. Proper orthogonal decomposition

3.1. *An overview of the POD*

At the core of the theoretical and experimental application of the POD is the replacement of the instantaneous random velocity by deterministic functions which have maximal projection on it. These deterministic functions (or eigenfunctions) are obtained either analytically or empirically from the resulting integral equation, the kernel of which is the two-point correlation of the velocity itself. The original field can be recovered by summing together (or integrating over) the contributions of each eigenfunction and its random coefficient, the latter determined by projecting each eigenfunction onto the instantaneous field (exactly like the determination of coefficients in ordinary Fourier analysis). Note that this projection and reconstruction requires that all points be measured simultaneously, which was not possible in this experiment. Thus only the eigenspectra and eigenvectors can be produced using rakes of probes as employed herein.

The turbulent axisymmetric wake is both stationary in time and homogeneous and periodic in the azimuthal direction. The POD integral equations can be immediately solved in these directions to yield Fourier modes, continuous in temporal frequency, f, and discrete in azimuthal mode number, m (George 1988, 1999). The streamwise direction is problematical, since it is neither homogenous nor of finite total energy. Hence in the absence of other considerations (like similarity), the eigenfunctions will be determined by how the domain is truncated. This problem is avoided in this study by only applying the POD to cross-sections of the flow, and treating the streamwise position, x, as a parameter. This particular version of the POD is sometimes called the 'slice' POD. The methodology applied here is identical to one of those applied to the axisymmetric jet by Jung *et al.* (2004) (see especially the appendices) and Gamard *et al.* (2004); the reader is referred to those papers for the details.

3.2. *This application*

If only the streamwise velocity component at a fixed downstream location, say x, is considered, the following integral equation(s) must be solved:

$$\int_0^S R_{x,x}(m, f, r, r'; x)\psi^{(n)}(m, f, r'; x)r' \,\mathrm{d}r' = \lambda^{(n)}(m, f; x)\psi^{(n)}(m, f, r; x) \tag{3.1}$$

where S is the limit of the domain, $R_{x,x}(m, f, r, r'; x)$ is the two-point velocity correlation Fourier transformed in time and expanded in Fourier series in the azimuthal direction, $\psi^{(n)}(m, f, r; x)$ are the eigenfunctions, and $\lambda^{(n)}(m, f; x)$ the corresponding eigenspectra. The eigenspectra, $\lambda^{(n)}(m, f; x)$, are representations of how the energy is distributed as a function of azimuthal mode number, m, and frequency, f, at a given downstream position, x. Therefore their downstream evolution shows how the main characteristics of the streamwise component of the turbulent kinetic energy evolve. The eigenfunctions, $\psi^{(n)}(m, f, r; x)$, are the basis functions for the flow.

It is important to first discuss what the variable f means, or more precisely, what it does *not* mean. Experimentally it is the frequency (or temporal variation) observed by the measuring apparatus. Its interpretation as space or time is complicated by the fact that the turbulence is being convected by the probes while it is also evolving in time. The so-called 'Taylor's frozen field hypothesis' assumes that convection dominates the temporal evolution, so that temporal variations can be interpreted as spatial variations. For the wake where $u'/U < 10\,\%$, Taylor's hypothesis is certainly valid, at least for all but the very lowest frequencies. Thus the proper interpretation of the frequency in this experiment, for all but the very lowest frequencies, is as a wavenumber, $k = 2\pi f/U$, where U is the local mean velocity. Because of the interesting problem at very low frequencies of the eigenspectra presented later in this paper, and the questionable applicability of Taylor's hypothesis for them, the data have been left in terms of the primitive variable, f.

In practice, the following steps are taken to implement the POD in this experiment:

(a) Measure the instantaneous velocity at two points.

(b) Fourier transform in time and compute the cross-spectrum.

(c) Repeat step (a) and (b) for many pairs of points.

(d) Expand the cross-spectra obtained in (b) in a Fourier series in the azimuthal direction.

(e) Solve the remaining eigenvalue problem in the radial direction, equation (3.1), for each frequency and azimuthal mode number.

This is exactly the procedure used by Glauser & George (1987) in their jet mixing layer study, and in an earlier version of this investigation of the axisymmetric wake by Johansson *et al.* (2002). It can be contrasted with the approach used by Citriniti & George (2000) where 138 probes were used to measure all positions simultaneously, thereby allowing reconstruction of the instantaneous field.

Due to the cylindrical coordinate system, r' is present inside the integral in equation (3.1). From a computational point of view, it is desirable to have the kernel Hermitian symmetric (Baker 1977). This can be achieved by separating r' into $r'^{1/2} \times r'^{1/2}$, and by multiplying the entire equation by $r^{1/2}$, then redefining the kernel to be $r^{1/2} R_{x,x}(m, f, r, r'; x) r'^{1/2}$ and the basis function $\psi^{(n)}(m, f, r; x) r^{1/2}$. The only effect of this operation is to simplify the computation, and there is no effect on the result.

The general symmetry properties of axisymmetric shear flows are treated in Gamard *et al.* (2004). In Appendix C, the specific properties of the kernel $R_{x,x}$ for the axisymmetric wake are presented. The results can be briefly summarized as follows: the eigenspectra, $\lambda^{(n)}(m, f; x)$ are the same in all four quadrants, i.e. quadrant II ($m > 0,\ f < 0$), quadrant III ($m < 0,\ f < 0$), and quadrant IV ($m < 0,\ f > 0$) are the same as quadrant I ($m > 0,\ f > 0$). The eigenfunctions differ slightly in that they are the same in quadrants I and IV, while in I and III they are complex conjugates, as they are in quadrants II and IV. Because of this, only data for $m > 0,\ f > 0$ are presented below.

4. POD results: eigenvalues

The distribution of the resolved energy in the POD modes is summarized in table 1. After $x/D \approx 50$, the first (radial) POD mode accounts for about 56 % of the total resolved energy, the second for about 19 %, the third for about 10 %, and the rest the remainder. Clearly the lowest-order POD mode dominates the energetics of the flow. This was expected from the Hilbert–Schmidt theory which applies to this direction, and produces ordered and proper results (the lowest order has the most energy, the

	$\lambda^{(n)}$							Energy
x/D	$n=1$	$n=2$	$n=3$	$n=4$	$n=5$	$n=6$	$n=7$	(10^{-5} m^2 s^{-2})
30	63.1	17.6	10.4	5.6	2.3	0.68	0.3	22.649
50	59.6	17.2	10.1	6.0	3.8	2.2	1.1	16.114
70	57.4	17.5	10.2	6.2	4.3	2.9	1.6	12.694
90	55.9	18.4	10.3	6.3	4.4	3.0	1.6	11.020
110	55.9	18.8	10.5	6.1	4.3	2.8	1.6	9.4162
130	56.7	18.6	10.4	6.0	4.0	2.7	1.5	8.2688
150	56.7	19.1	10.2	6.0	4.0	2.6	1.3	7.1374

TABLE 1. Relative percentage per POD mode number, and total turbulent kinetic energy resolved.

next the next most, etc.). For the remainder of this paper, it is this lowest-order POD mode ($n=1$) and its associated eigenspectrum, $\lambda^{(1)}(m, f; x)$, which will receive most of the attention.

4.1. *The eigenspectra as functions of m and f*

Figure 2 shows three-dimensional plots of the first eigenspectrum, $\lambda^{(1)}(m, f; x)$, for the disk wake at $x/D = 30$, 50, 70, 90, 110, 130 and 150. The most striking feature is the clear separation of the frequency content of the various modes. Only mode-1 has a peak at a non-zero frequency. The other eigenspectra (of which mode-2 is predominant) all resemble the usual broadband one-dimensional spectra of turbulence which peak at zero frequency (usually due to aliasing from the unresolved directions). The eigenspectra have not been normalized, so their heights decay downstream as the wake itself decays. But even from just these seven plots it is obvious that mode-1 dies more quickly than the other modes, and especially mode-2. In fact, the reason for the behaviour of the normalized azimuthal mode number plots below (figure 7) is clearly not that mode-2 is increasing its contribution, but that mode-1 is fading more rapidly.

This can be seen in another way as illustrated in figure 3. The value of $\lambda^{(1)}(m, f; x)$ for which it has a local maximum is plotted as a function of downstream distance for each of azimuthal modes 0, 1, and 2. Clearly azimuthal mode-1 is dying out faster than the others, at least for the first 100 or so diameters downstream.

The downstream evolution of the azimuthal modes can be seen even more clearly in figure 4. Here, slices of the surface plots in figure 2 are shown for fixed azimuthal mode numbers $m = 0$, 1, and 2 as a function of frequency. As in figure 2, the eigenspectra have not been normalized.

Figure 5 shows plots of the total energy and azimuthal mode-1 alone as a function of frequency for the same downstream positions. Most striking is that the peak frequency of the band which contains most of the energy for azimuthal mode-1 does not evolve downstream, but is fixed. Moreover its contribution to the total energy is clearly diminishing downstream, as noted above. Thus the primary contribution of azimuthal mode-1 clearly does not scale in local shear layer variables, but is instead determined only by the Strouhal number of the near wake. It seems apparent that the primary contribution to azimuthal mode-1 has been convected in from the near wake, and is virtually independent of the local shear layer of the wake.

By contrast, the behaviour of azimuthal mode-2 is quite different. Figure 6 shows azimuthal mode-2 normalized by the energy remaining after the energy from azimuthal

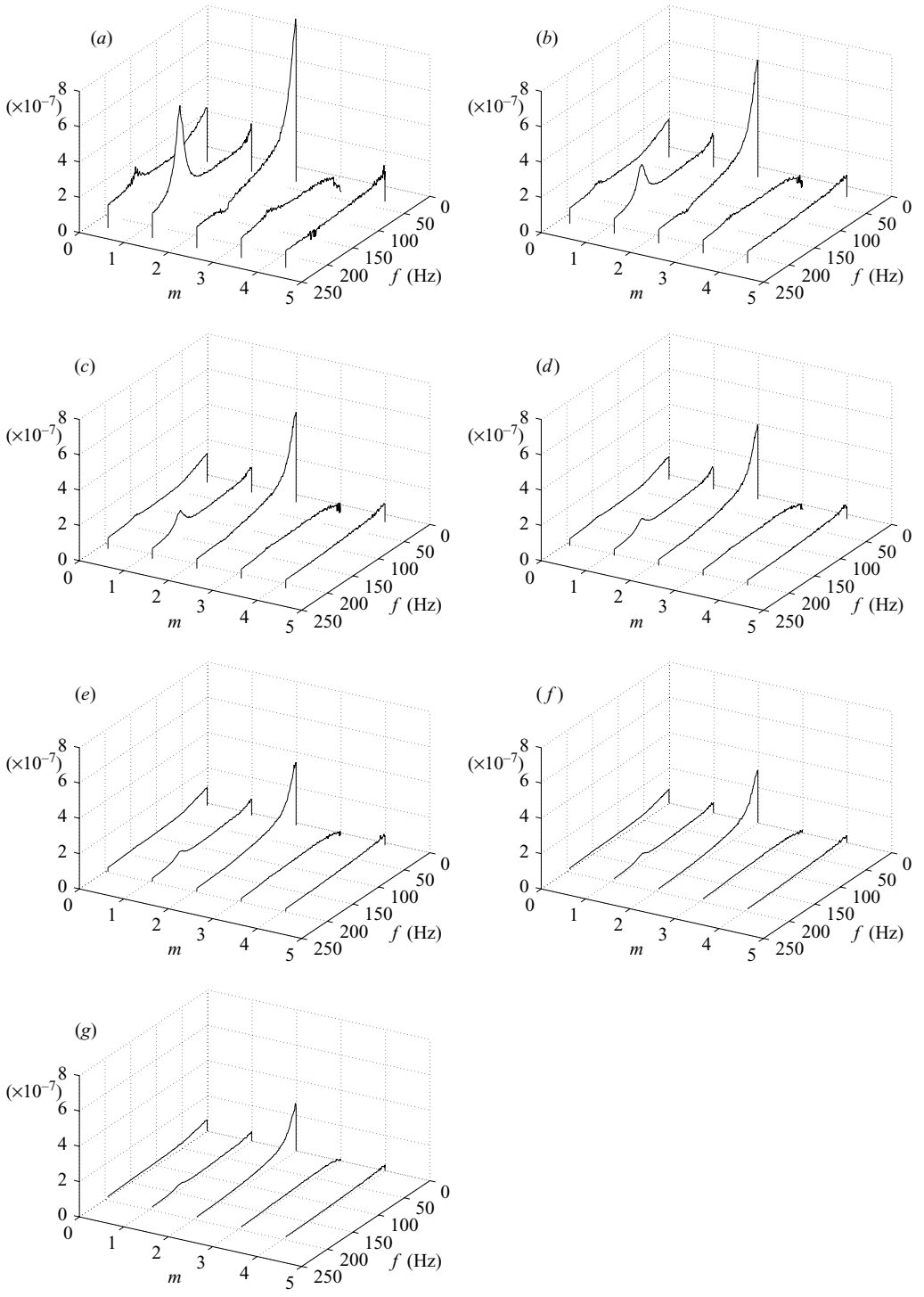

FIGURE 2. Eigenspectrum, $\lambda^{(1)}(m, f; x)$, as function of azimuthal mode number, m, and frequency, f, at different positions: (*a*) $x/D = 30$, (*b*) 50, (*c*) 70, (*d*) 90, (*e*) 110, (*f*) 130, and (*g*) 150.

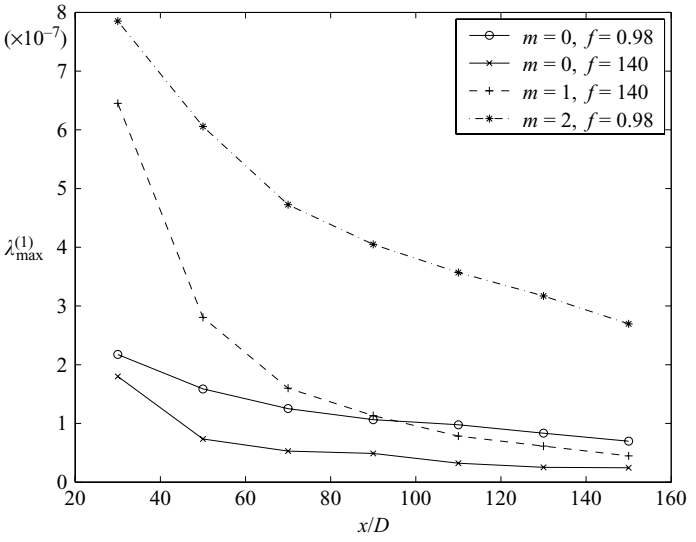

FIGURE 3. Maximum values of λ.

mode-1 is removed. These data have been plotted as wavenumber spectra using Taylor's frozen field hypothesis. Note the remarkable 'notch' in azimuthal mode-2 (all the way to zero) for the position closest to the disk at exactly the frequency where azimuthal mode-1 is dominant. Clearly azimuthal mode-1 is suppressing the development of azimuthal mode-2 at the dominant frequency. As the wake develops downstream, this notch fills in, and except for the very lowest wavenumbers (for which Taylor's hypothesis is of doubtful validity), these data collapse very well in shear layer variables. Thus, once the contribution of azimuthal mode-1 has been removed, the rest of the turbulence behaves exactly as might be expected from an equilibrium similarity wake (see George 1989 or Johansson, George & Gourlay 2003). This is certainly not the case if azimuthal mode-1 is not removed, which explains the frustrations of many authors in trying to explain their measurements for this flow.

4.2. *Eigenvalues integrated over frequency*

The eigenspectra can be integrated over frequency, f, to obtain the distribution of energy with only the azimuthal mode number, m. If this is normalized by the total energy at the cross-section the result is

$$\xi^{(1)}(m;x) = \frac{\displaystyle\int_0^\infty \lambda^{(1)}(m,\, f;x)\,\mathrm{d}f}{\displaystyle\sum_{m=0}^{M}\int_0^\infty \lambda^{(1)}(m,\, f;x)\,\mathrm{d}f} \tag{4.1}$$

where M is the highest resolved azimuthal mode. Figure 7 shows the evolution of the eigenspectra integrated over frequency as a function of the azimuthal mode number. For the near wake, at $x/D = 10$, azimuthal mode-1 dominates, exactly as reported by others (Fuchs *et al.* 1979; Berger *et al.* 1990). But by $x/D = 30$, the energy in azimuthal mode-2 is nearly equal to that in azimuthal mode-1. By $x/D = 50$, azimuthal mode-2 dominates, as it does for all positions downstream. The difference between modes 0

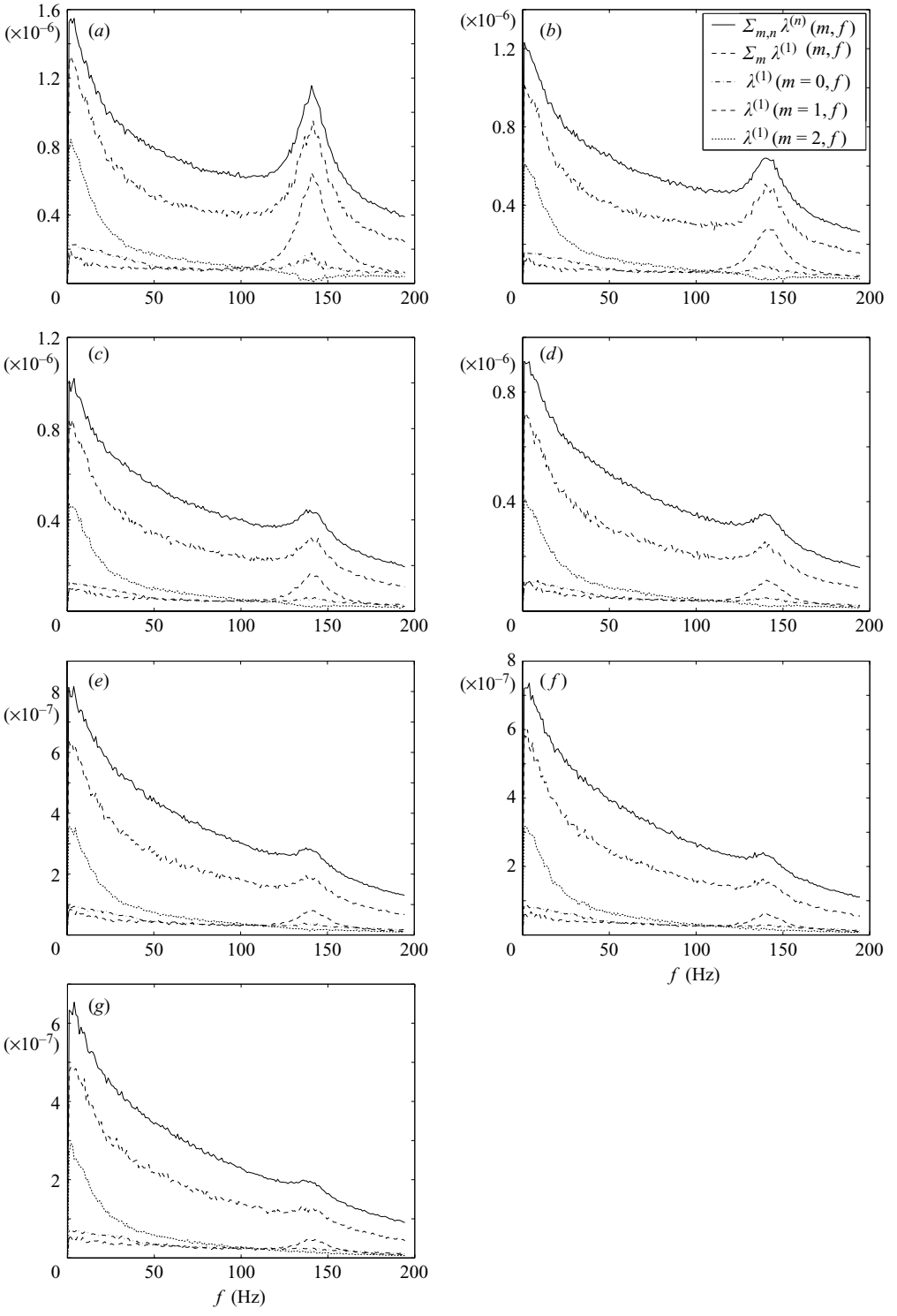

FIGURE 4. Slices of the eigenspectrum, $\lambda^{(1)}(m, f; x)$, as function of azimuthal mode number, m, and frequency, f, at different positions: (*a*) $x/D = 30$, (*b*) 50, (*c*) 70, (*d*) 90, (*e*) 110, (*f*) 130, and (*g*) 150.

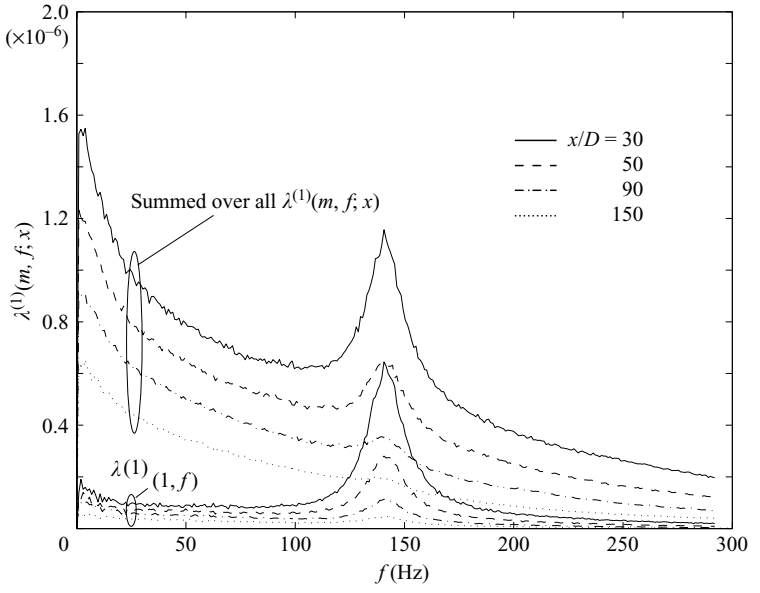

FIGURE 5. The total energy and mode-1 alone as a function of frequency at $x/D = 30$, 50, 90 and 150.

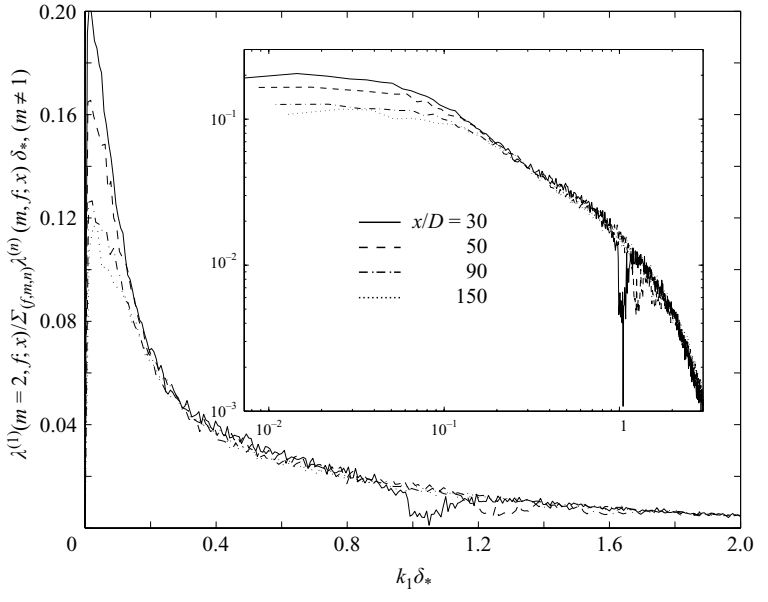

FIGURE 6. Mode-2 at $x/D = 30$, 50, 90 and 150, normalized by the energy remaining after the energy from mode-1 is removed. These data have been plotted as wavenumber spectra using Taylor's hypothesis.

and 1 far downstream is too small to be certain which is the largest, since the slight variation may be due to the differing areas covered by the probe arrays as the wake grows (as discussed in Appendix A).

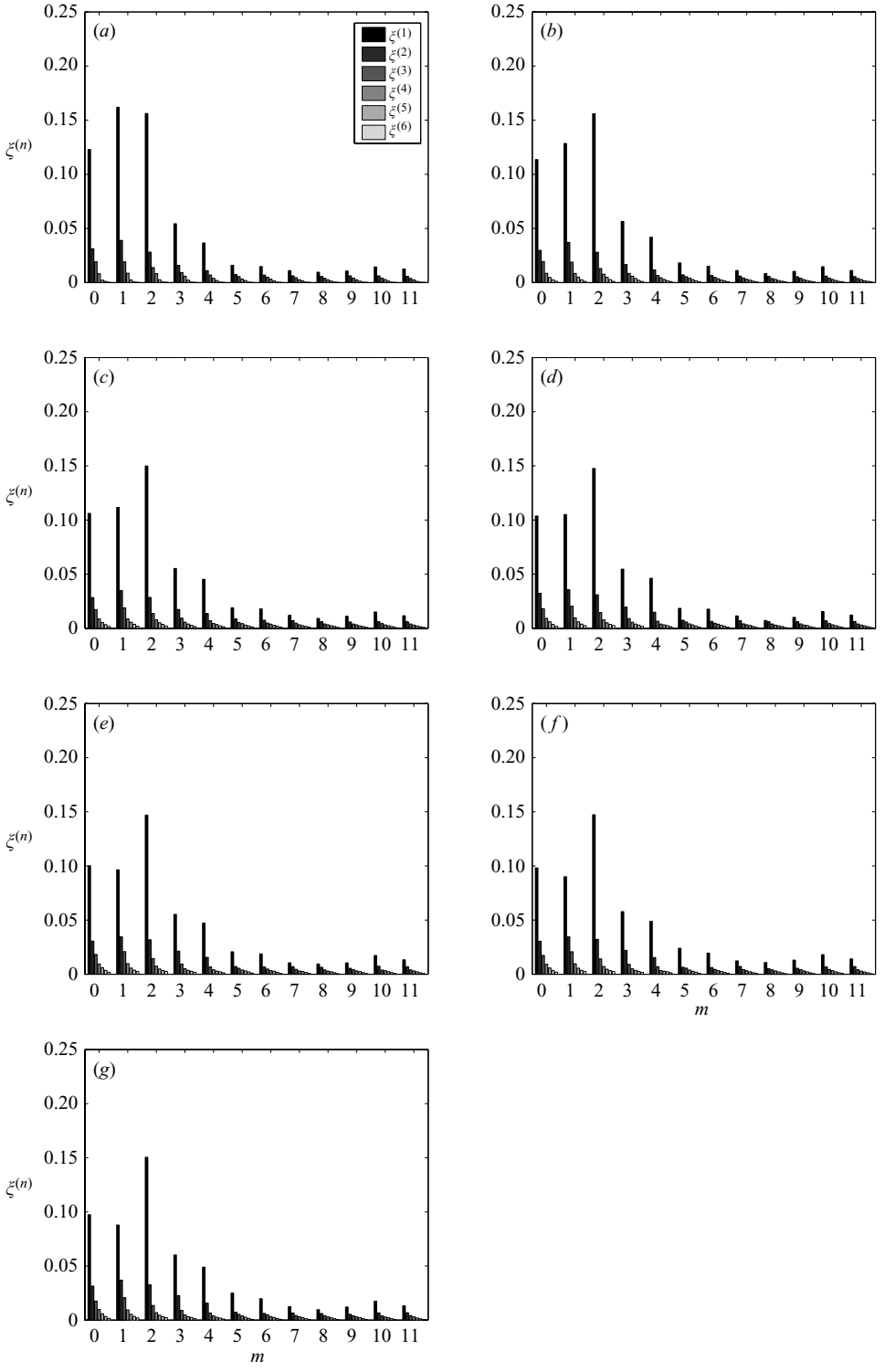

FIGURE 7. Eigenspectrum integrated over frequency (as defined in equation (4.1)) as a function of azimuthal mode number (m) at different positions: (a) $x/D = 30$, (b) 50, (c) 70, (d) 90, (e) 110, (f) 130, and (g) 150.

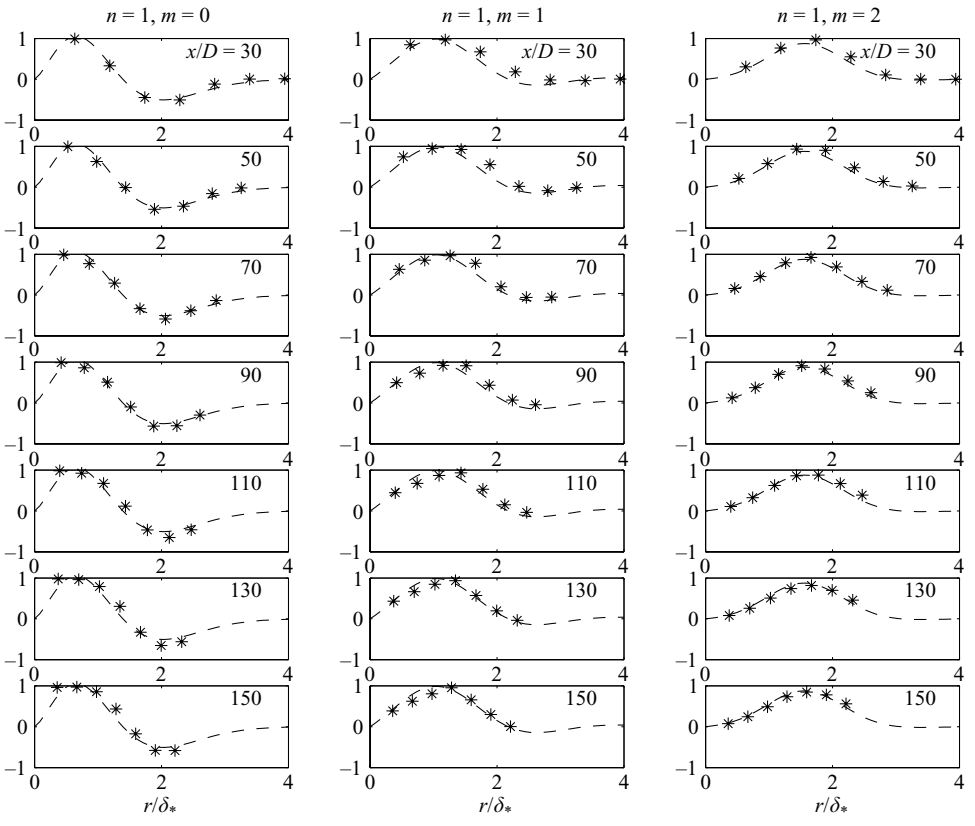

FIGURE 8. Eigenfunctions for the first POD mode, $r^{1/2}\psi^{(1)}(m, f, r; x)$, and the first three azimuthal modes ($m = 0, 1, 2$) vs. r/δ_*.

5. POD results: eigenfunctions

The eigenfunctions, $\psi^{(n)}(m, f, r; x)$, can be viewed as being the basic functions or the building blocks of the flow and the eigenvalues indicate which eigenfunctions are most important in terms of kinetic energy. The larger the eigenvalue, the more important is the associated eigenfunction. As is clear from the results presented in § 4, almost all activity was found for azimuthal modes 0, 1 and 2. Hence only the corresponding eigenfunctions are treated here. For the eigenvalues, for each azimuthal mode, an eigenfunction is found for each frequency. This in general complicates the display of results, but surprisingly the shapes of the eigenfunctions were found to be almost completely independent of frequency.

Due to the axisymmetric configuration in this application it is most convenient to work with $\psi^{(n)}(m, f, r; x)\, r^{1/2}$ since the integral equation (3.1) then becomes Hermitian symmetric as discussed in § 3. Thus all figures display $\psi^{(n)}(m, f, r; x)\, r^{1/2}$.

The eigenfunctions for the first POD mode and azimuthal modes 0, 1, and 2 are shown in figure 8. The eigenfunctions are in general complex, but it was found that the imaginary part was negligible. Furthermore, there is one eigenfunction for each frequency (f), azimuthal mode number (m), and POD mode number (n). It was found that there was very little variation with frequency, so all results were averaged over frequency. A virtually identical result would have been found if one arbitrarily chosen frequency, but averaging was applied to avoid selecting a particular frequency.

In Part 1 scaling properties were determined and presented; so here the radial coordinate is scaled with the transverse length scale δ_*. Since the probe rake used in the experiment was fixed and the wake grows it is clear from figure 8 that different parts of the wake are covered as the probe rake was traversed downstream. At $x/D = 30$ the inner part is relatively poorly resolved while the entire wake is covered. At $x/D = 150$ the situation is reversed with the inner part being well resolved and the outer part of the wake located outside the probe rake. The effect of probe array coverage on the results is discussed in Appendix A but in fact no observable dependence of array coverage was found. This is manifested in figure 8 by remarkably similar eigenfunctions for all downstream positions.

The experimentally obtained eigenfunctions are denoted with an asterisk. The dashed line is a nonlinear curve fit consisting of a fourth-order polynomial times an exponential function with a second-order polynomial in the argument. One curve was fitted for each azimuthal mode number and for each POD mode number (n). The curve was fitted to all downstream locations simultaneously.

For POD-mode $n = 1$ and for azimuthal mode $m = 0$ it is clear from figure 8 that the eigenfunction has a positive peak near $r/\delta_* = 1$ and a negative peak further out in the flow, near $r/\delta_* = 2$. The pattern is not the same for azimuthal modes $m = 1$ and 2, which only exhibit a positive peak. For $m = 1$ the peak is located between $r/\delta_* = 1$ and 2 and for $m = 2$ the peak is located further out closer to $r/\delta_* = 2$. This can be interpreted as azimuthal mode $m = 0$ being active and present in the whole cross-section, while the actions of the higher-order azimuthal modes take place away from the centre. This is consistent with the view that azimuthal mode $m = 1$ is associated with periodic vortex shedding at the Strouhal frequency, an event detectable in ordinary power spectra only away from the centre of the wake as shown in Part 1.

For higher-order POD modes, the situation is depicted in figures 9 and 10. Figure 9 shows that for POD mode $n = 2$, there is a very small dependence on azimuthal modes. In all positions downstream, every eigenfunction has one negative and one positive peak, the first being closer to the centre of the wake. The peak location seems to shift outwards, even though the effect is hardly noticeable, for increasing azimuthal mode number.

Figure 10 show the eigenfunctions for POD mode $n = 3$. Here the situation is similar to that for POD mode $n = 2$ in that it is also noticeable how similar the eigenfunctions are for all azimuthal modes. The most distinguishing feature of the POD mode $n = 3$ eigenfunctions are that there are now two positive peaks and one negative peak: thus the number of zero-crossings increases by one with increasing POD mode number, consistent with the idea of "sequency" (R. Adrian 2003, private communication to W. K. G.).

6. Discussion

As presented above, the modal decomposition of the turbulent axisymmetric wake can be viewed as being composed by two major features: azimuthal modes 1 and 2. Initially, azimuthal mode 1 dominates the modal decomposition. This mode dies out rapidly and no longer dominates the flow after $x/D = 30$. Even so, it continues to be visible in the modal decomposition for all downstream positions covered in this study. This mode is associated with the Strouhal peak in the power spectra, presented in Part 1. The behaviour of mode-1 is consistent with findings of Cannon *et al.* (1993), who stated that this feature remains in the wake for very large downstream distances. In their azimuthal decomposition at $x/\theta = 105$, they actually noticed mode-1 to be

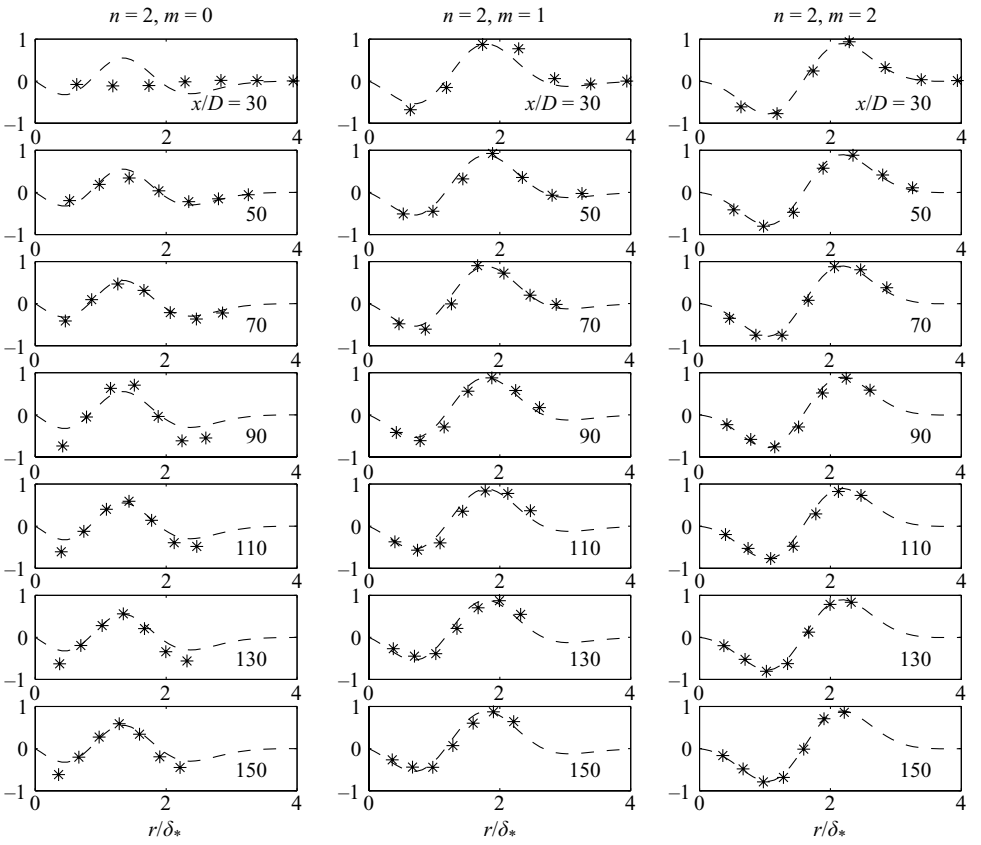

FIGURE 9. Eigenfunctions for the second POD mode $r^{1/2}\psi^{(2)}(m, f, r; x)$, and the first three azimuthal modes ($m = 0, 1, 2$) vs. r/δ_*.

the most prominent mode. But it must be noted that their decomposition was made at a single radial position in the wake, unlike the POD applied here which takes the whole cross-section of the flow into consideration.

One additional observation can be made from figure 3. There is a very interesting problem presented by the lack of collapse of the spectra for azimuthal mode-2 at very low wavenumbers (or perhaps just low frequencies). These very large scales clearly satisfy Townsend's idea of the large eddies. They contain about 5–10 % of the energy and do not appear to interact with the main motion. If these data are not normalized as wavenumbers, but simply by the energy present at all mode numbers with mode-1 removed, they collapse without any scaling of the frequency axis at all. So what is their role, if any? This is not at all clear at the time of writing. One possibility is that they simply slowly twist the mean flow. If so this could account for the remarkably high local turbulence intensity for this flow for which at the centreline $u'/(U_\infty - U_{CL}) \approx 110\,\%$. In effect, the mean profile could be simply moved around by this very large and slow modulation. There is some evidence for this in the flow visualizations of Taneda (1978) who observed wave-like behaviour of the wake. Also, some of the azimuthally averaged instantaneous DNS profiles of Gourlay *et al.* (2001) appear to be slightly off-centre, consistent with both observations above.

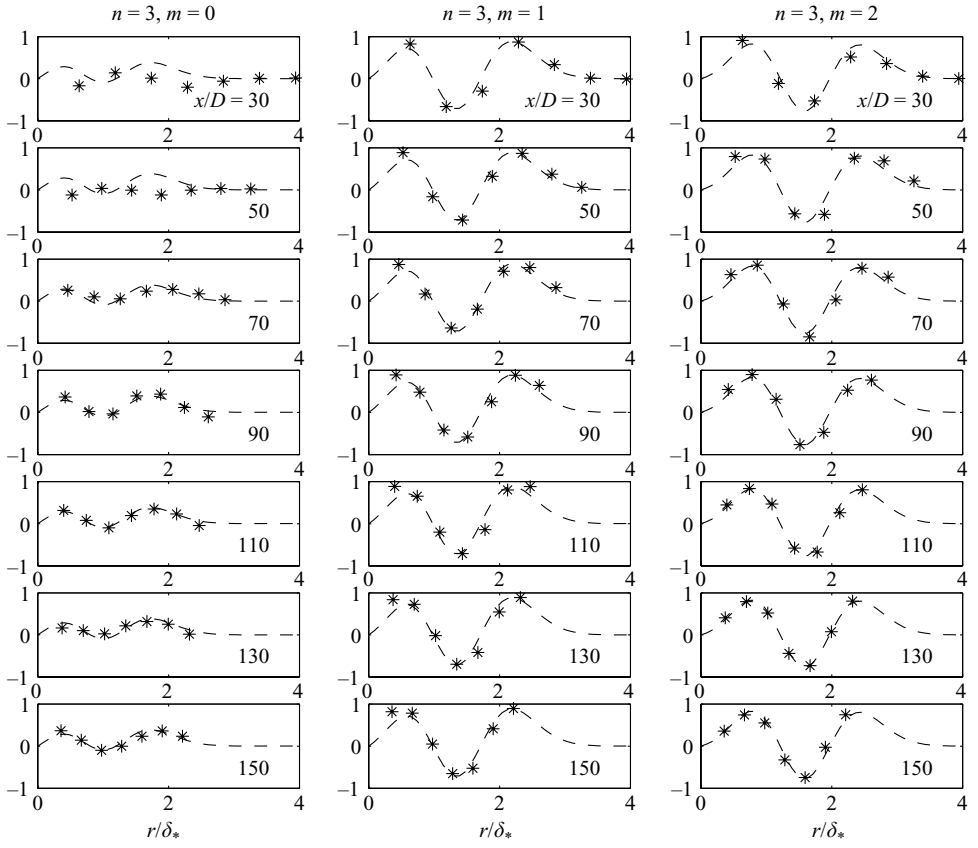

FIGURE 10. Eigenfunctions for the third POD mode, $r^{1/2}\psi^{(3)}(m, f, r; x)$, and the first three azimuthal modes ($m = 0, 1, 2$) vs. r/δ_*.

It is also worth commenting on what the usual conditional sampling approaches to coherent structures have focused on for this flow. The single most coherent energetic motion is the transient azimuthal mode-1, and this is indeed what such studies have yielded. But this is the least important part of the problem for the far wake, since it is dying out and appears to be virtually independent of the rest of the turbulence. Similar considerations apply to the jet as well where the most apparent coherent feature of the near jet flow (mode 0) has seemingly nothing to do with the far jet's evolution, but is simply dying out, see Gamard *et al.* (2002).

Like the jet, the emergence of this mode-2 dominance also corresponds to the emergence of the similarity state, particularly evident in the normalized turbulence intensity which does not approach a constant until about $x/D = 30$–50. The implications of this for studies of axisymmetric wakes are profound, since most attempts seldom measured much beyond this point (e.g. Cannon 1991; Uberoi & Freymuth 1970) due to the extremely low turbulence intensities of the wake, and the demands on wind tunnel quality and test section length.

7. Conclusions

The high-Reynolds-number axisymmetric wake behind a disk has been studied from $x/D = 30$ to $x/D = 150$ using the proper orthogonal decomposition (POD). It

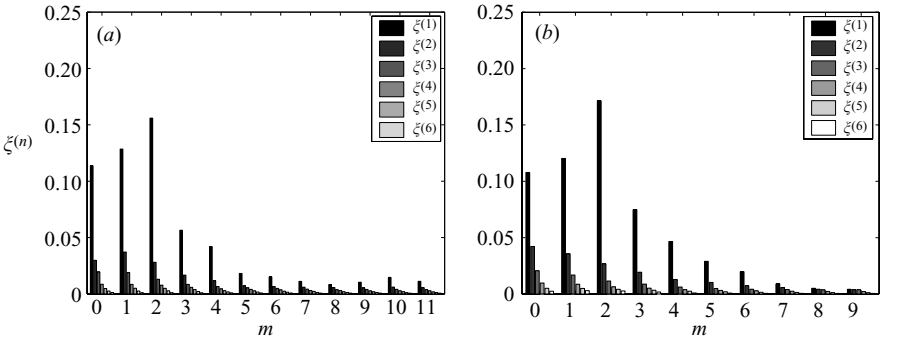

FIGURE 11. Eigenspectrum integrated over frequency as function of azimuthal mode number (m) at $x/D = 50$ for different configurations: (a) 15 hot wires, (b) 13 hot wires.

was found that the energetic structure of the axisymmetric wake can efficiently be described in terms of a few POD modes with the first radial POD mode containing approximately 56 % of the energy. Two features dominated the eigenspectra, manifested as major peaks. The first peak is an azimuthal mode 1 peak at a frequency corresponding to the Strouhal number of the wake. The second is an azimuthal mode-2 peak at near-zero frequency. The mode-1 peak dies out faster than the mode-2 peak, so that the far wake is dominated by the latter.

This evolution from azimuthal mode-1 dominance in the near wake to mode-2 dominance in the far wake corresponds closely to the approach to equilibrium similarity. Once mode-2 becomes equally as important as mode-1 (after $x/D = 30$ or $x/\theta = 110$), the ratio of turbulence intensity to centreline velocity deficit is constant, the mean deficit and turbulence intensity collapse in similarity variables, and the wake grows as $x^{1/3}$.

The authors would like to thank Professor Henrik Alfredsson of the Swedish Royal Institute of Technology (KTH) for the use of the their MTL windtunnel. The first author would also especially like to thank Mr. Davide Medici for sharing the tunnel time and for the company during the experiment. Professors Jöran Bergh (Chalmers), Jean-Paul Bonnet (U. Poitiers) Dan Ewing (McMaster U.) and Jonathan Naughton (U. Wyoming) provided very useful comments, for which we are grateful. As well we appreciate the many contributions of our colleagues, especially Dr Stephan Gamard throughout the investigation and Mr Elteyeb Eljack near the end. This work was initially supported by Chalmers University of Technology. It continues with the support of the Swedish Research Council, grant number 2641.

Appendix A. Effect of array coverage

Figure 11 shows the wake at $x/D = 50$ from our experiment described in the main text, together with the data obtained with the 13-wire rake and four support wires presented in Johansson *et al.* (2002). There are only very small differences, one being that mode 0 is slightly larger for the 15-wire rake. This can be explained by the fact that this rake covers a larger portion of the wake. However, this effect is very small.

Figure 12 shows plots of ru^2 versus r for all downstream positions. The total energy in the POD is the integral under these curves. Clearly as the rake is traversed downstream, progressively less and less of the total energy is included in the decomposition (since the hot-wire rake is fixed). (This was one of the primary reasons for expanding

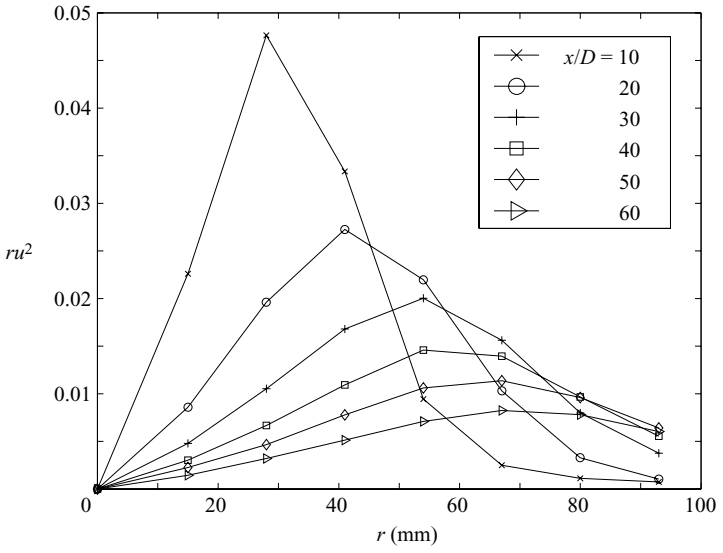

FIGURE 12. ru^2 vs. r at various downstream positions.

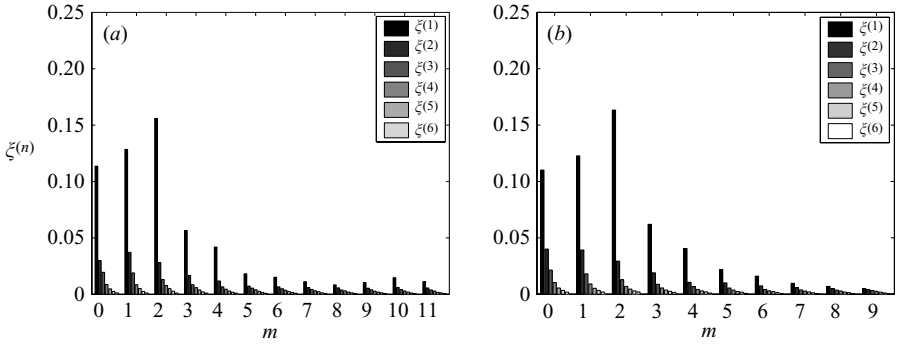

FIGURE 13. Eigenspectrum integrated over frequency as function of azimuthal mode number (m) at $x/D = 50$ for different configurations: (a) 3 pairs of support wires, (b) 4 pairs of support wires.

from 13 to 15 wires.) The energy lost is less than 1 % at $x/D = 10$ but perhaps as much as 20 % at $x/D = 60$. As figure 7 makes clear, the evolution from an azimuthal mode-1 peak to a peak at mode-2 takes place between $x/D = 30$ and 40. Beyond $x/D = 40$ there is virtually no change in the eigenspectra, even though progressively more of the energy is lost. This suggests strongly that the external energy does not affect the eigenspectra (at least in the lower modes). This is consistent with the lack of differences observed between the 13- and 15-wire arrays.

Appendix B. Effect of disk support wires

Figure 13 shows plots for the four- and three-wire supported rakes, obtained using the 15-hot-wire rake at $x/D = 50$. The results are virtually indistinguishable, suggesting strongly that the whatever the physical cause of the observations, it is not a consequence of how the disk is supported in the wind tunnel.

Appendix C. Symmetry considerations for statistically axisymmetric wakes without swirl

Jung *et al.* (2004) show that the following relations are general for the 1-1 cross-spectrum of any axisymmetric flow which is statistically stationary in time, homogeneous and periodic in the azimuthal direction, and apply here for all values of m including $m=0$:

$$R_{x,x}(x, r, r'; -m, -f) = R_{x,x}(x, r', r; m, f). \tag{C 1}$$

Alternatively, since the cross-correlation itself is real, it follows immediately that

$$R_{x,x}(x, r, r'; -m, -f) = R^*_{x,x}(x, r, r'; m, f). \tag{C 2}$$

Thus the values of $R_{x,x}$ in the third quadrant ($m < 0$, $f < 0$) can be found from those in the first by simply interchanging r and r' of the cross-spectrum for positive values, or by taking the complex conjugate.

Similarly

$$R_{x,x}(x, r, r', -m, f) = R_{x,x}(x, r', r, m, -f) \tag{C 3}$$

and

$$R_{x,x}(x, r, r', -m, f) = R^*_{x,x}(x, r, r', m, -f) \tag{C 4}$$

indicating that if the cross-spectrum is known for $m<0$, $f>0$ then the values for $m>0$, $f<0$ can be obtained by either interchanging r and r' or taking the complex conjugate, or vice versa.

Thus, stationarity in t and homogeneity in the azimuthal direction, θ, imply that the doubly transformed cross-spectra in quadrants I ($m>0$, $f>0$) and III ($m<0$, $f<0$) are related, and that quadrants II ($m>0$, $f<0$) and IV ($m<0$, $f>0$) are related. There is in general no relation between quadrants I and II (or IV). Thus, in the absence of additional information or constraints, the cross-spectrum $R_{x,x}(x, r, r', m, f)$ must be specified in at least two quadrants of m and f.

For all of the wake experiments reported herein, however, it was possible to establish from the measured cross-spectra that to within experimental error, the following additional symmetry condition applied:

$$R_{x,x}(x; r, r', m, -f) = R^*_{x,x}(x; r, r', m, f). \tag{C 5}$$

One example is shown in figure 14. Note that equation (C 5) does not apply to all statistically axisymmetric flows and applies only to the wake (and perhaps not even to all wakes); for example it does not apply to the axisymmetric jet, which appears to satisfy a different condition (cf. Jung *et al.* 2004).

When added to the general constraints above, it is easy using the same methodology to show that this supplies the missing condition to obtain the cross-spectra in quadrants II, III, and IV in terms of the information in quadrant I alone. For example, consider the eigenvalue problem posed by

$$\int_D R_{x,x}(x; r, r', m, -f)\psi^{(n)}(x, r', m, -f) r' \,\mathrm{d}r' = \lambda^{(n)}(m, -f; x)\psi^{(n)}(x, r, m, -f). \tag{C 6}$$

Using equation (C 5) this becomes

$$\int_D R^*_{x,x}(x; r, r', m, f)\psi^{(n)}(x, r', m, -f) r' \,\mathrm{d}r' = \lambda^{(n)}(m, -f; x)\psi^{(n)}(x, r, m, -f). \tag{C 7}$$

By taking the complex conjugate and recognizing that the λ are real, it follows immediately that the solutions to this equation must be the same as for the original

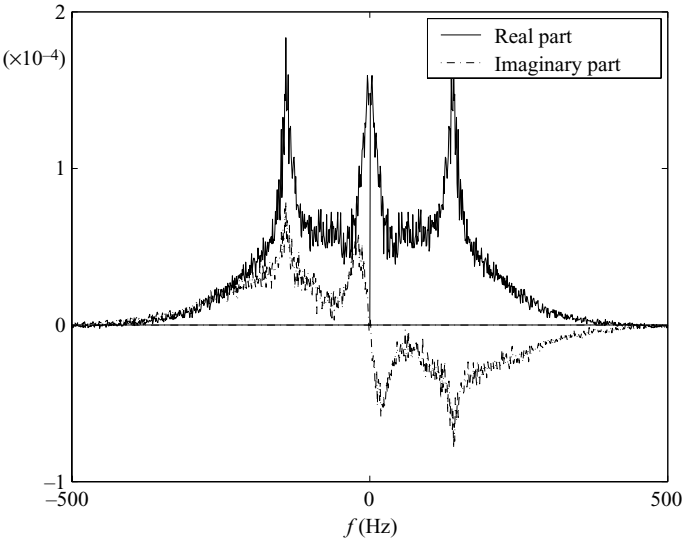

FIGURE 14. $R_{x,x}(x, r, r', m, f)$ for $x/D = 30$, $m = 0$, $r = 1$ and $r' = 2$.

problem posed by equation (3.1). Therefore the following must be true:

$$\lambda^{(n)}(m, -f; x) = \lambda^{(n)}(m, f; x), \tag{C 8}$$

$$\psi^{*(n)}(x, r, m, -f) = \psi^{(n)}(x, r, m, f). \tag{C 9}$$

Thus the values in quadrant II ($m > 0$, $f < 0$) are the complex conjugates of those in quadrant I. It is similarly easy to show that the eigenspectra must be the same in all quadrants, while the eigenfunctions in quadrants II and III are the complex conjugates of those in I and IV respectively. Hence only quadrant I data are shown in the body of the paper.

Interestingly, and unlike the jet, it is also straightforward to show that equation (C 5) implies that the two-point correlation transformed over frequency *is* only symmetrical in the separation angle, ϑ, as commonly assumed. It can be reconstructed from the Fourier series representation of $R_{x,x}(x, r, r', \vartheta, f)$ as follows:

$$B_{x,x}(x, r, r', \vartheta, f) = \sum_{m=-\infty}^{\infty} \mathrm{e}^{+\mathrm{i}m\vartheta} R_{x,x}(x, r, r', m, f) \tag{C 10}$$

This can be rewritten as a sum over positive values of m only as

$$B_{x,x}(x, r, r', \vartheta, f) = R_{x,x}(x, r, r', 0, f) + \sum_{m=1}^{\infty} \left\{ \mathrm{e}^{+\mathrm{i}m\vartheta} R_{x,x}(x, r, r', m, f) + \mathrm{e}^{-\mathrm{i}m\vartheta} R_{x,x}(x, r, r', -m, f) \right\}. \tag{C 11}$$

From equations (C 4) and (C 5) it follows immediately that

$$\begin{aligned} B_{x,x}(x, r, r', \vartheta, f) &= R_{x,x}(x, r, r', 0, f) \\ &\quad + \sum_{m=1}^{\infty} \left\{ \mathrm{e}^{+\mathrm{i}m\vartheta} R_{x,x}(x, r, r', m, f) + \mathrm{e}^{-\mathrm{i}m\vartheta} R^{*}_{x,x}(x, r, r', m, -f) \right\} \\ &= R_{x,x}(r, r', 0, f) + 2 \sum_{m=1}^{\infty} R_{x,x}(x, r, r', m, f) \cos m\vartheta. \end{aligned} \tag{C 12}$$

Clearly $B_{x,x}(r, r', \vartheta, f)$ is an even function of ϑ, and therefore symmetrical in ϑ.

It is not clear at the time of writing why equation (C 5) is true. Therefore in the absence of a theoretical explanation it should be regarded as tentative. An important clue may lie in the fact that the axisymmetric jet appears to satisfy a different condition, suggesting that the unique character of each flow is at least reflected in this difference, if indeed not determined by it.

REFERENCES

Baker, C. T. H. 1977 *The Numerical Treatment of Integral Equations*. Clarendon.

Batchelor, G. K. & Gill, E. A. 1962 Analysis of the instability of axisymmetic jets. *J. Fluid Mech.* **14**, 529–551.

Berger, E., Scholz, D. & Schumm, M. 1990 Coherent vortex structures in the wake of a sphere and a circular disk at rest and under forced vibrations. *J. Fluids Struct.* **4**, 231–257.

Bonnet, J. P., Delville, J., Glauser, M. N., Antonia, R. A., Bisset, D. K., Cole, D. R., Fiedler, H. E., Garem, J. H., Hilberg, D., Jeong, J., Kevlahan, N. K. R., Ukeiley, L. S. & Vincendeau, E. 1998 Collaborative testing of eddy structure identification methods in free turbulent shear flows. *Exps. Fluids* **25**, 197–225.

Cannon, S., Champagne, F. & Glezer, A. 1993 Observations of large-scale structures in wakes behind axisymmetric bodies. *Exps. Fluids* **14**, 447–450.

Cannon, S. C. 1991 Large-scale structures and the spatial evolution of wakes behind axisymmetric bluff bodies. PhD thesis, Dept. of Aerospace and Mechanical Engineering, University of Arizona.

Citriniti, J. H. & George, W. K. 2000 Reconstruction of the global velocity field in the axisymmetric mixing layer utilizing the proper orthogonal decomposition. *J. Fluid Mech.* **418**, 137–166.

Delville, J., Ukeiley, L., Cordier, L., Bonnet, J. P. & Glauser, M. 1999 Examination of large-scale structures in a turbulent plane mixing layer. Part 1. Proper orthogonal decomposition. *J. Fluid Mech.* **391**, 91–122.

Freund, J. F. & Colonius, T. 2002 POD analysis of sound generation by a turbulent jet. *AIAA Paper* 2002–0072.

Fuchs, H. V., Mercker, E. & Michel, U. 1979 Large scale coherent structures in the wake of axisymmetric bodies. *J. Fluid Mech.* **93**, 189–211.

Gamard, S., Jung, D. & George, W. K. 2004 Downstream evolution of the most energetic modes in a turbulent axisymmetric jet at high reynolds number. Part 2. The far jet. *J. Fluid Mech.* **514**, 205–230.

Gamard, S., Jung, D., Woodward, S. & George, W. K. 2002 Application of a 'slice' POD to the far field of an axisymmetric turbulent jet. *Phys. Fluids* **14** (7), 2515–2522.

George, W. K. 1988 Insight into the dynamics of coherent structures from a proper orthogonal decomposition. In *Proc. Symposium on Near Wall Turbulence*, *Dubrovnik, Yugoslavia.* (ed. S. Kline), pp. 168–180. Hemisphere.

George, W. K. 1989 The self-preservation of turbulent flows and its relation to initial conditions and coherent structures. In *Advances in Turbulence* (ed. W. K. George & R. E. A. Arndt), pp. 39–73. Hemisphere.

George, W. K. 1999 Some thoughts on similarity, the POD, and finite boundaries. In *Fundamental Problematic Issues in Turbulence* (ed. A. Gyr, W. Kinzelbach & A. Tsinober), pp. 117–128. Birkhauser.

George, W. K., Johansson, P. B. V. & Gamard, S. 2002 How has the study of coherent structures contributed to our understanding of turbulent free shear flows? In *2002 ASME Fluid Engineering Division Summer Meeting*, *Montreal, Canada, July 14–18.*

Ghidersa, B. & Dušek, J. 2000 Breaking of axisymmetry and onset of unsteadiness in the wake of a sphere. *J. Fluid Mech.* **423**, 33–69.

Glauser, M. & George, W. 1987 Orthogonal decomposition of the axisymmetric jet mixing layer including azimuthal dependence. In *Advances in Turbulence* (ed. G. Comte-Bellot & J. Mathieu), pp. 357–366. Spring.

Glauser, M. N. 1987 Coherent structures in the axisymmetric turbulent jet mixing layer. PhD thesis, State University of New York at Buffalo.

Glauser, M. N. & George, W. K. 1992 Application of multipoint measurements for flow characterization. *Exp. Therm. Fluid Sci.* **5**, 617–632.

Gourlay, M. J., Arendt, S. C., Fritts, D. C. & Werne, J. 2001 Numerical modeling of initially turbulent wakes with net momentum. *Phys. Fluids* **13**, 3783–3802.

Johansson, A. V. 1992 A low speed wind-tunnel with extreme flow quality – design and tests. In *Prog. ICAS Congress 1992*, pp. 1603–1611. ICAS-92-3.8.1.

Johansson, P. B. V. & George, W. K. 2006 The far downstream evolution of the high-Reynolds-number axisymmetric wake behind a disk. Part 1. Single-point statistics. *J. Fluid Mech.* **555**, 363–385.

Johansson, P. B. V., George, W. K. & Gourlay, M. J. 2003 Equilibrium similarity, effects of initial conditions and local Reynolds number on the axisymmetric wake. *Phys. Fluids.* **15** (3), 603–617.

Johansson, P. B. V., George, W. K. & Woodward, S. H. 2002 Proper orthogonal decomposition of an axisymmetric turbulent wake behind a disk. *Phys. Fluids* **14** (7), 2508–2514.

Johnson, T. A. & Patel, V. C. 1999 Flow past a sphere up to a reynolds number of 300. *J. Fluid Mech.* **378**, 19–70.

Jung, D., Gamard, S. & George, W. K. 2004 Downstream evolution of the most energetic modes in a turbulent axisymmetric jet at high Reynolds number. Part 1. The near field region. *J. Fluid Mech.* **514**, 173–204.

Kim, I. & Pearlstein, A. J. 1990 Stability of the flow past a sphere. *J. Fluid Mech.* **211**, 73–93.

Lee, S. I. & Bearman, P. W. 1992 An experimental investigation of the wake structure behind a disk. *J. Fluids Struct.* **6**, 437–450.

Lumley, J. L. 1967 The inertial subrange in nonequilibrium turbulence. In *Atmospheric Turbulence and Radio Wave Propagation* (ed. A. M. Yaglom & V. I. Tatarsky), pp. 157–164. Moscow, USSR: Nauka.

Magarvey, R. H. & Bishop, R. L. 1961 Transition ranges for three-dimensional wakes. *Can. J. Phys.* **39**, 1418–1422.

Magarvey, R. H. & MacLatchy, C. S. 1965 Vortices in sphere wakes. *Can. J. Phys.* **43**, 1649–1656.

Marshall, D. & Stanton, T. E. 1931 On the eddy system in the wake of flat circular plates in three dimensional flow. *Proc. R. Soc. Lond.* A **130**, 295–301.

Miau, J. J., Leu, T. S., Liu, T. W. & Chou, J. H. 1997 On vortex shedding behind a circular disk. *Exps. Fluids* **23**, 225–233.

Möller, W. 1938 Experimentelle untersuchengen zur hydrodynamik der kugel. *Phys. Z.* **39**, 57–80.

Monkewitz, P. A. 1988 A note on vortex shedding from axisymmetric bluff bodies. *J. Fluid Mech.* **192**, 561–575.

Natarajan, R. & Acrivos, A. 1993 The instability of the steady flow past spheres and disks. *J. Fluid Mech.* **254**, 323–344.

Pao, H.-P. & Kao, T. W. 1977 Vortex structure in the wake of a sphere. *Phys. Fluids* **20** (2), 187–191.

Perry, A. E. & Lim, T. T. 1978 Coherent structures in coflowing jets and wakes. *J. Fluid Mech.* **88**, 451–463.

Perry, A. E. & Watmuff, J. H. 1981 The phase-averaged large-scale structures in three-dimensional turbulent wakes. *J. Fluid Mech.* **103**, 33–51.

Roberts, J. B. 1973 Coherence measurements in an axisymmetric wake. *AIAA J.* **11**, 1569–1571.

Sato, H. & Okada, O. 1966 The stability and transition of an axisymmetric wake. *J. Fluid Mech.* **26**, 237–253.

Taneda, S. 1978 Visual observations of the flow past a sphere at Reynolds numbers between 10^4 and 10^6. *J. Fluid Mech.* **85**, 187–192.

Tomboulides, A. G. & Orszag, S. A. 2000 Numerical investigation of transitional and weak turbulent flow past a sphere. *J. Fluid Mech.* **416**, 45–73.

Uberoi, M. S. & Freymuth, P. 1970 Turbulent energy balance and spectra of the axisymmetric wake. *Phys. Fluids* **13** (9), 2205–2210.